Carbonate weathering as a driver of carbon dioxide supersaturation in lakes

***in press* in Nature Geoscience(_16/12/14)**

Rafael Marcé[1*†], Biel Obrador[2†], Josep-Anton Morguí[2,3], Joan Lluís Riera[2], Pilar López[2], Joan Armengol[2]

[1] Catalan Institute for Water Research (ICRA), Emili Grahit 101, 17003 Girona, Spain

[2] Department of Ecology, University of Barcelona, Diagonal 643, 08028 Barcelona, Spain

[3] Catalan Institute of Climate Sciences (IC3), Doctor Trueta 203, 08005 Barcelona, Spain

*Corresponding author: rmarce@icra.cat

[†] These two authors contributed equally to this paper

1

Most lakes and reservoirs are known to have surface carbon dioxide concentrations that are supersaturated relative to the atmosphere[1], and the resulting carbon dioxide emissions represent a substantial flux of the continental carbon balance[2–4]. Therefore, unravelling the drivers of carbon dioxide supersaturation in lakes is necessary for a proper understanding of the land carbon cycle and its sensitivity to external perturbations[4–6]. Carbon dioxide supersaturation has generally been attributed to a widespread imbalance of lake net ecosystem production towards net heterotrophy[7,8], but recent findings challenge this interpretation[9–11]. Here we show that considering inputs of dissolved inorganic carbon from carbonate weathering substantially improves our understanding of the processes leading to carbon dioxide supersaturation. We used simple metabolic models to analyze water chemistry data from a survey of reservoirs covering a wide range of lithologies to reveal that carbon dioxide supersaturation in lakes with alkalinity above 1 meq L^{-1} is directly related to carbonate weathering. Then, we evaluate the worldwide distribution of alkalinity in lakes and show that 57% of the area occupied by lakes and reservoirs is above 1 meq L^{-1}. Remarkably, carbon dioxide emissions related to carbonate weathering are relevant in tropical and temperate latitudes, but negligible in boreal regions.

There are two main mechanisms leading to carbon dioxide (CO_2) supersaturation in lakes and reservoirs: 1) in situ net ecosystem production (NEP) imbalanced towards net heterotrophy[7] (i.e., respiration exceeding photosynthesis); and 2) inputs of groundwater or surface water with high dissolved inorganic carbon (DIC) content coming from both weathering of minerals and soil respiration in the watershed[10–14]. Among these, NEP is usually considered to be the main factor driving CO_2 supersaturation in lakes[7,8]. However, most studies relating CO_2 supersaturation to NEP have focused on relatively dilute, low-

alkalinity lakes, despite the fact that CO_2 concentration in water is strongly modulated by the carbonate equilibrium (i.e., the chemical reactions relating the different forms of DIC). Therefore, we lack conclusive evidence of the impact of NEP on CO_2 supersaturation in a range of systems showing contrasting DIC content.

To test how DIC content can drive CO_2 supersaturation and modulate the relationship between NEP and CO_2 concentration, we use data from a nation-wide study[15] including 202 measurements of dissolved oxygen (DO), DIC, alkalinity, and CO_2 concentration in the surface layer of a set of Spanish reservoirs covering a wide range of DIC content and trophic states (Supplementary Table 1 and Supplementary Data). We use the observed DO disequilibrium relative to the atmosphere as a surrogate for surface lake NEP, and investigate its impact on observed DIC and CO_2 concentrations considering three metabolic models. The models combine assumptions concerning the DIC loading from the watershed and the effect of lake NEP (Fig. 1a). All three models assume that the DIC generated during weathering of minerals in the watershed (DIC^W) dominates DIC loading to the lake, but while in Model 1 DIC^W inputs are in equilibrium with the atmosphere before entering the lake, Models 2 and 3 assume no equilibration. Additionally, we consider a potential linkage between NEP and precipitation and dissolution of carbonate minerals (e.g., calcium carbonate) in Model 3. Although little is known about the relevance of reactions with carbonate minerals on lake CO_2 supersaturation at regional scales, exchange of inorganic carbon between the DIC pool and carbonate minerals has potential effects on CO_2 supersaturation[16-18].

The observed data set shows a linear relationship between DO and DIC disequilibrium relative to the atmosphere (Fig. 1b), scattered around the 1:1 line. A factorial regression analysis for alkalinity ($P<0.001$) indicates that this linear relationship shows significant intercepts above zero and milder slopes as alkalinity increases (Fig. 1b). Model 1 does not

account for this pattern (Fig. 1c), because it can only produce a single line with zero intercept and a slope following the 1:1 stoichiometry. Model 2 produces DO versus DIC disequilibrium relationships with increasing intercept as alkalinity increases (Fig. 1c), but all lines show a 1:1 dependency on DO disequilibrium at odds with observations. In contrast, Model 3 mimics the behaviour of the observational set (Fig. 1d), and explains a considerably greater amount of DIC disequilibrium variability (R^2=40%, 43%, and 79% for Models 1, 2, and 3, respectively, n=202), suggesting that both DIC^W and the links between precipitation of carbonates and NEP may modulate NEP effects on DIC.

There are two principal consequences embedded in Model 3 that challenge the customary link between CO_2 supersaturation and net heterotrophy. First, sensitivity of CO_2 supersaturation to DO disequilibrium weakens as alkalinity increases (Fig. 2a), to the extent that it is possible to find both CO_2 and DO supersaturation (suggesting photosynthesis exceeds respiration) in samples with alkalinity higher than 1 meq L^{-1} (Fig. 2b). These patterns are consistent with our dataset and also with recent findings in lakes across USA[10]. These results are not at odds with our hypothesis that precipitation of carbonates may contribute to the lower sensitivity of CO_2 supersaturation to DO disequilibrium at high alkalinity (Fig. 2), which is also consistent with the observed calcium carbonate saturation (Supplementary Fig. 1). Precipitation of carbonates is a well known phenomenon in inland waters[17,18], and it is intimately linked to NEP in the ocean[19]. Moreover, there is growing evidence that carbonate precipitation can be linked to NEP in both benthic[18] and planktonic[20] freshwater compartments. However, we lack direct evidence of carbonate precipitation in our lakes, and other factors potentially affecting the relationship between NEP and CO_2 supersaturation like differential atmospheric exchange and anaerobic metabolism[21], while unlikely in the surface waters of our deep systems, cannot be ruled out (Supplementary Methods). Therefore, additional direct evidences on the effect of carbonate reactions on lake CO_2 supersaturation should be obtained to reach a solid conclusion.

79 The second and more fundamental consequence of Model 3 is that large CO_2
80 supersaturation can be found even at DO equilibrium relative to the atmosphere in systems
81 with alkalinity higher than 1 meq L^{-1} (Fig. 2b). The relationship between CO_2
82 supersaturation and alkalinity is strongly dependent on water temperature (insert in Fig.
83 2b), and the alkalinity needed to reach CO_2 supersaturation at DO equilibrium considerably
84 rises above 1 meq L^{-1} at colder temperatures (e.g., 2.6 meq L^{-1} at 5ºC), indicating that the
85 impact of alkalinity on CO_2 supersaturation is unlikely in lakes located at high latitudes. In
86 our model the coupling between CO_2 supersaturation and alkalinity at NEP=0 rests on the
87 assumption that DIC inputs from the watershed are equivalent to DIC^W, which implies that
88 the DIC input reaches the lake as if soil respiration inputs and atmospheric exchanges
89 balanced each other during DIC transport through river networks. This is not at odds with
90 the current understanding that soil-derived CO_2 degases rapidly in headwater streams[2,22].
91 Even though this assumption may be inadequate to understand the dynamics of a particular
92 system, assuming that DIC^W dominates DIC loading from the watershed allows for a
93 satisfactory description of CO_2 supersaturation across a population of lakes. However, this
94 assumption is more likely to hold in systems showing higher alkalinity, because in those
95 systems DIC^W can be very large in relation to DIC changes promoted by soil respiration
96 and degassing. In low alkalinity waters even modest DIC inputs from soil respiration will
97 lead to marked shifts in CO_2 concentration. This seems to be the case in our dataset, where
98 large CO_2 supersaturation are found in some low alkalinity (<1 meq L^{-1}) samples showing
99 DO disequilibrium close to 0 (insert in Fig. 2b), clearly differing from the range of CO_2
100 supersaturation predicted by our model. This suggests alternative DIC sources other than
101 DIC^W driving CO_2 supersaturation at NEP=0 in low alkalinity waters, most probably soil
102 respiration[11,22].

103 Our results suggest that CO_2 supersaturation is independent of in situ NEP in many lakes,
104 and that a significant amount of the carbon evaded through their surface may be directly

105 related to weathering of minerals in the watershed that supply alkalinity to surface waters.
106 To evaluate the relevance of these results at the global scale, we elaborated a global map of
107 alkalinity in runoff and merged it with a spatially explicit global lake and reservoir
108 database[23,24], in order to obtain global estimates of alkalinity across lakes (Methods). The
109 empirical cumulative distribution functions of alkalinity for lakes and reservoirs are similar
110 (Fig. 3a), and show that 57% and 34% of the area occupied by lakes and reservoirs
111 corresponds to systems with alkalinity higher than 1 and 2 meq L^{-1}, respectively. The
112 prevalence of systems showing alkalinity values above the threshold for acute effects on
113 CO_2 supersaturation is even higher in some carbonate-rich regions (Fig. 3b). Between
114 latitudes 30-50°N (including most USA, the Mediterranean, and extensive areas in Asia)
115 and 10-20°S (which comprise the large African lakes) more than half of the area occupied
116 by lakes shows alkalinity values above 2 meq L^{-1}. Thus, the role of carbonate weathering on
117 CO_2 supersaturation should be overlooked neither at global nor at regional scales.

118 Although with our database it is difficult to disentangle the separate roles of DIC^W and in
119 situ NEP on CO_2 supersaturation, we can estimate the potential global CO_2 emissions from
120 weathering of minerals using our assumption that DIC^W arrives at lakes without substantial
121 equilibration with the atmosphere. From the global distribution of lakes and reservoirs and
122 our global alkalinity map, CO_2 emissions of a lake at NEP=0 are calculated from the
123 corresponding DIC^W and assuming a temperature dependent gas exchange velocity[3]
124 (Methods). The CO_2 emissions calculated in this way roughly correspond with the potential
125 emissions from the supply of alkalinity to lakes and reservoirs, and amounts to 0.09 Pg C
126 yr^{-1} or 35.3 g C m^{-2} yr^{-1}, a considerable fraction (between 12 and 33%) of recent estimates
127 of carbon emissions from lakes (106 to 300 g C m^{-2} yr^{-1})[2–4,25]. It also represents a
128 considerable fraction of the 0.5 Pg C yr^{-1} attributed to carbon supply from weathering
129 reactions[4]. Interestingly, the relevance of weathering-related carbon emissions can be very
130 different across latitudes (Fig. 3b,c). While DIC^W can potentially account for half of the

emissions in tropical and temperate latitudes, it is negligible in boreal regions, due to both lithologies producing little alkalinity and low temperatures that hamper CO_2 supersaturation (insert in Fig. 2b). Remarkably, our estimate of the relevance of DIC^W for lake CO_2 emissions in temperate latitudes (ca. 50%) is similar to the relevance of soil-derived CO_2 for carbon emissions in streams and rivers of the conterminous USA (up to 32%)[26].

The irrelevant role of DIC^W in boreal lakes explains the high sensitivity of CO_2 supersaturation to lake NEP found in systems located in Precambrian shields[27], a result that fuelled the customary link between CO_2 supersaturation and in situ NEP in the literature[7,8]. However, our results imply that this rule does not necessarily apply in systems receiving substantial loads of alkalinity from the watershed, and contribute to explain the apparent mismatch between the global prevalence of net heterotrophy (ca. 50%) and CO_2 supersaturation (ca. 90%) in lakes[8,28]. The role of alkalinity is also crucial to predict the seasonal evolution of CO_2 supersaturation in response to seasonal NEP variability, a current gap in global CO_2 emissions estimates from lakes[2]. Indeed, our dataset shows a marked seasonal evolution of CO_2 supersaturation, but this seasonality is hampered at high alkalinity (Supplementary Fig. 2), suggesting that CO_2 will remain supersaturated in those lakes except in very productive situations during the growing season (Fig. 2a). Finally, our results open the question of how anthropogenic impacts on weathering rates[29] can affect CO_2 emissions from lakes in temperate regions, and whether deforestation and other land use changes in tropical latitudes can deliver alkalinity stored in the organic soil layers[30], potentially increasing alkalinity-driven CO_2 emissions.

Methods

In situ measurements of DO, alkalinity, and pH were performed in the surface layer of 101 reservoirs across Spain during two field trips in winter 1987 and summer 1988. The reservoirs were included in a regional limnological program[15] and were selected to cover a wide range of alkalinity and trophic states to account for the diverse lithology of the Iberian Peninsula. CO_2 and DIC concentrations were calculated from alkalinity and pH (Supplementary Methods). For regression analyses, the data set was split into three groups using the 33% and 66% alkalinity percentiles: low alkalinity (n = 67, median = 0.4, range = 0.06-0.83 meq L^{-1}), mid alkalinity (n = 68, median = 1.6, range = 0.88-2.22 meq L^{-1}), and high alkalinity (n = 67, median = 3.0, range = 2.27-4.69 meq L^{-1}). Analyses using raw data and Box-Cox transformed variables to account for deviations from normality rendered identical results (Supplementary Methods).

The three metabolic models assume a 1:1 mol stoichiometry between DO and DIC concentration during metabolism. Model 1 predicts observed DIC concentration as:

$$DIC = DIC^{NEP=0} - NEP \quad (1)$$

$DIC^{NEP=0}$ (μmol C L^{-1}) is the DIC concentration before in-lake NEP effects. Assumptions to calculate $DIC^{NEP=0}$ are fundamental because we do not have measures for the initial state before NEP effects (represented in the model by the DO disequilibrium relative to the atmosphere, μmol O_2 L^{-1}). In Model 1 we assumed that this reference state is the equilibrium with the atmosphere, and $DIC^{NEP=0}$ was calculated as the DIC of a sample with the measured alkalinity and dissolved CO_2 corresponding to atmospheric equilibrium. This

176 is equivalent to say that the reference state is the DIC coming from weathering of minerals
177 in the watershed (DIC^{W}) after equilibration with the atmosphere.

178 Model 2 only differs from Model 1 in the assumptions used to calculate the reference state.
179 In this case $DIC^{NEP=0} = DIC^{W}$, being DIC^{W} = alkalinity. This is equivalent to assert that the
180 reference state is the DIC coming from weathering of minerals in the watershed (DIC^{W})
181 without equilibration with the atmosphere.

182 Model 3 adds a term to account for precipitation and dissolution of carbonates:

183

184 $$DIC = DIC^{NEP=0} - NEP - \alpha\, NEP \quad (2)$$

185

186 where the term αNEP accounts for DIC exchanged during the reversible reaction (positive
187 towards $CaCO_3$ precipitation):

188

189 $$Ca^{2+} + 2HCO_3^- \leftrightarrow CaCO_3 + CO_2 + H_2O \quad (3)$$

190

191 Note that we used calcium carbonate as a convenient example, but the reaction may
192 involve any cation precipitating as a carbonate mineral. In equation (2) α is the molar ratio
193 between precipitation and dissolution of carbonates and NEP. α values for freshwater
194 systems are almost absent in the literature beyond the fact that calcification is unlikely at
195 alkalinity below 1 meq L^{-1} (ref. 18). Thus, we considered α=0 for samples showing
196 alkalinity below 1 meq L^{-1}. For alkalinity above this value, we defined two groups separated
197 by an arbitrary alkalinity threshold located at the 66% percentile of the observed alkalinity
198 distribution in our database (2.23 meq L^{-1}). We assumed α=0.6 above this threshold, and
199 α=0.2 below it (ref. 18 and Supplementary Methods). We assessed the sensitivity of our

200 results to the choice of α by performing 1000 simulations with random combinations of α
201 values. Model 3 was always the best model in terms of explained variability of observed
202 DIC disequilibrium irrespective of α values.

203 The global distribution of lake alkalinity was estimated by overlapping existing global geo-
204 referenced datasets of lakes and reservoirs[23,24] with a global map of alkalinity in runoff. The
205 global alkalinity map was elaborated from relationships between runoff and alkalinity
206 generation considering different lithologies and solving the routing of alkalinity through the
207 global river network (Supplementary Methods and Supplementary Fig. 3). Large lakes were
208 treated separately in this analysis using bibliographical data, because no lithology was
209 assigned in the regions defined by their margins. To calculate CO_2 emissions from the
210 input of alkalinity to lakes and reservoirs we calculated the CO_2 concentration
211 corresponding to a sample with the corresponding alkalinity in a closed system
212 (Supplementary Methods). We assumed a gas exchange velocity and its dependence on
213 temperature as in Ref. 3, to have a reference value of global CO_2 emission from lakes to
214 which compare our estimations of alkalinity-driven potential emissions (Supplementary
215 Methods).

References

1. Cole, J. J., Caraco, N. F., Kling, G. W. & Kratz, T. K. Carbon dioxide supersaturation in the surface waters of lakes. *Science* **265,** 1568–1570 (1994).

2. Raymond, P. A. *et al.* Global carbon dioxide emissions from inland waters. *Nature* **503,** 355–359 (2013).

3. Aufdenkampe, A. K. *et al.* Riverine coupling of biogeochemical cycles between land, oceans, and atmosphere. *Front. Ecol. Environ.* **9,** 53–60 (2011).

4. Regnier, P. *et al.* Anthropogenic perturbation of the carbon fluxes from land to ocean. *Naure Geosci.* **6,** 597–607 (2013).

5. Richey, J. E., Melack, J. M., Aufdenkampe, A. K., Ballester, V. M. & Hess, L. L. Outgassing from Amazonian rivers and wetlands as a large tropical source of atmospheric CO_2. *Nature* **416,** 617–620 (2002).

6. Luyssaert, S. *et al.* The European carbon balance. Part 3: forests. *Glob. Chang. Biol.* **16,** 1429–1450 (2010).

7. Cole, J. J., Pace, M. L., Carpenter, S. R. & Kitchell, J. F. Persistence of net heterotrophy in lakes during nutrient addition and food web manipulations. *Limnol. Oceanogr.* **45,** 1718–1730 (2000).

8. Duarte, C. M. & Prairie, Y. T. Prevalence of heterotrophy and atmospheric CO_2 emissions from aquatic ecosystems. *Ecosystems* **8,** 862–870 (2005).

9. Balmer, M. B. & Downing, J. Carbon dioxide concentrations in eutrophic lakes: undersaturation implies atmospheric uptake. *Inl. Waters* **1,** 125–132 (2011).

10. Mcdonald, C. P., Stets, E. G., Striegl, R. G. & Butman, D. Inorganic carbon loading as a primary driver of dissolved carbon dioxide concentrations in the lakes and reservoirs of the contiguous United States. *Global Biogeochem. Cycles* **27,** 285–295 (2013).

11. Maberly, S. C., Barker, P. A., Stott, A. W. & De Ville, M. M. Catchment productivity controls CO_2 emissions from lakes. *Nature Clim. Change* **3,** 391-394 (2013).

12. Bouillon, S. *et al.* Contrasting biogeochemical characteristics of the Oubangui River and tributaries (Congo River basin). *Sci. Rep.* **4,** 5402 (2014).

13. Stets, E. G., Striegl, R. G., Aiken, G. R., Rosenberry, D. O. & Winter, T. C. Hydrologic support of carbon dioxide flux revealed by whole-lake carbon budgets. *J. Geophys. Res.* **114,** G01008 (2009).

14. López, P., Marcé, R. & Armengol, J. Net heterotrophy and CO_2 evasion from a productive calcareous reservoir: Adding complexity to the metabolism-CO_2 evasion issue. *J. Geophys. Res.* **116,** G02021 (2011).

15. Riera, J. L., Jaume, D., de Manuel, J., Morguí, J. A. & Armengol, J. Patterns of variation in the limnology of Spanish reservoirs: A regional study. *Limnetica* **8,** 111–123 (1992).

16. Duarte, C. M. *et al.* CO_2 emissions from saline lakes: A global estimate of a surprisingly large flux. *J. Geophys. Res.* **113,** G04041 (2008).

17. Stabel, H. H. Calcite precipitation in Lake Constance: Chemical equilibrium, sedimentation, and nucleation by algae. *Limnol. Oceanogr.* **31,** 1081–1093 (1986).

18. McConnaughey, T. A. & Whelan, J. F. Calcification generates protons for nutrient and bicarbonate uptake. *Earth-Science Rev.* **42,** 95–117 (1997).

19. Riebesell, U. *et al.* Reduced calcification of marine plankton in response to increased atmospheric CO_2. *Science* **407,** 364–367 (2000).

20. Dittrich, M., Kurz, P. & Wehrli, B. The role of autotrophic picocyanobacteria in calcite precipitation in an oligotrophic lake. *Geomicrobiol. J.* **21,** 45–53 (2004).

21. Torgersen, T. & Branco, B. Carbon and oxygen dynamics of shallow aquatic systems: Process vectors and bacterial productivity. *J. Geophys. Res.* **112,** G03016 (2007).

22. Mayorga, E. *et al.* Young organic matter as a source of carbon dioxide outgassing from Amazonian rivers. *Nature* **436,** 538–41 (2005).

23. Lehner, B. & Döll, P. Development and validation of a global database of lakes, reservoirs and wetlands. *J. Hydrol.* **296,** 1–22 (2004).

24. Lehner, B. *et al.* High-resolution mapping of the world's reservoirs and dams for sustainable river-flow management. *Front. Ecol. Environ.* **9,** 494–502 (2011).

25. Barros, N. *et al.* Carbon emission from hydroelectric reservoirs linked to reservoir age and latitude. *Nature Geosci.* **4,** 593–596 (2011).

26. Butman, D. & Raymond, P. A. Significant efflux of carbon dioxide from streams and rivers in the United States. *Nature Geosci.* **4,** 839–842 (2011).

27. Lapierre, J. F., Guillemette, F., Berggren, M., del Giorgio, P. A. Increases in terrestrially derived carbon stimulate organic carbon processing and CO_2 emissions

in boreal aquatic ecosystems. *Nat. Commun.* **4,** 2972 doi: 10.1038/ncomms3972 (2013).

28. Hoellein, T. J., Bruesewitz, D. A. & Richardson, D. C. Revisiting Odum (1956): A synthesis of aquatic ecosystem metabolism. *Limnol. Oceanogr.* **58,** 2089–2100 (2013).

29. Raymond, P. A., Oh, N.-H., Turner, R. E. & Broussard, W. Anthropogenically enhanced fluxes of water and carbon from the Mississippi River. *Nature* **451,** 449–452 (2008).

30. Markewitz, D., Davidson, E. A., Figueiredo, R. de O., Victoria, R. L. & Krusche, A. V. Control of cation concentrations in stream waters by surface soil processes in an Amazonian watershed. *Nature* **410,** 802–805 (2001).

End notes

Acknowledgements. Financial support for this research was provided by projects CARBONET (Spanish Ministry, CGL201130474C020), and SCARCE (Consolider-Ingenio 2010 CSD2009-00065). We are grateful to Matthias Koschorreck, Núria Catalán, and Daniel von Schiller for comments on early drafts.

Author Contributions. R. M. and B. O. conceived the paper and contributed equally to this work; J. L. R. and J. A. M. obtained the reservoir data during the 1987-1988 survey; R. M. and B. O. analyzed the field data and R. M. performed worldwide computations; R. M. and B. O. co-wrote the paper. P. L. assisted in the interpretation of the data; J. A. designed and supervised the nation-wide sampling. All authors discussed the results and commented on the manuscript.

Additional information

Supplementary information is available in the online version of the paper. Reprints and permissions information is available online at www.nature.com/reprints. Correspondence and requests for materials should be addressed to R.M.

Competing financial interests

The authors declare no competing financial interests.

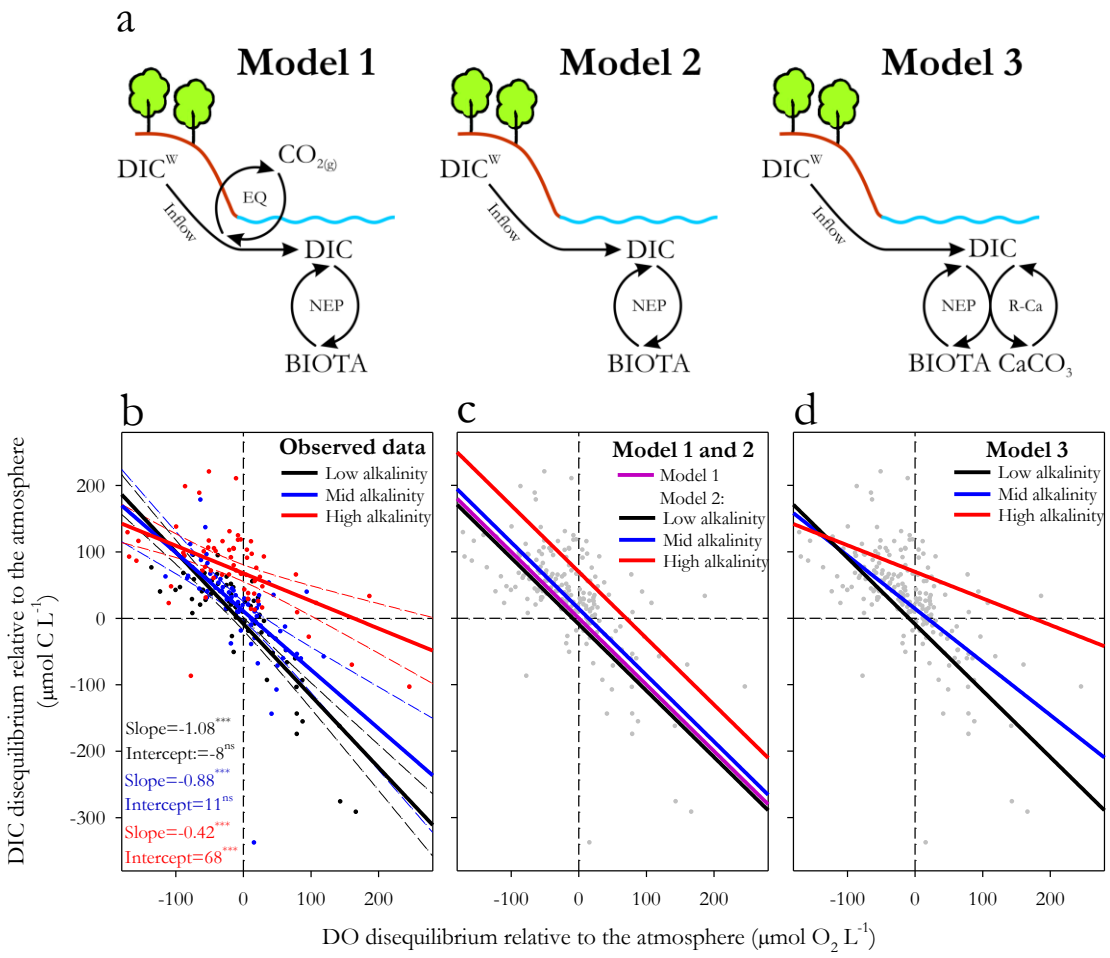

313

314 **Figure 1. DIC of lakes controlled by DIC inflow from the watershed and NEP. a,**

315 Conceptual representation of the three models considered to explain CO_2 supersaturation

316 in lakes. EQ=equilibration with the atmosphere. R-Ca=reactions with calcium carbonate

317 (Methods). **b-d,** Observed and modeled relationships between DO and DIC disequilibrium

318 relative to the atmosphere considering 3 alkalinity groups (Methods). **b,** Observed linear

319 relationships and 95% confidence intervals. ***P<0.0001, ns=non significant. **c,** Model 1

320 results and three realizations of Model 2 and **d,** three realizations of Model 3 using the

321 median values of the groups in **b**. Dots in grey are observed data.

322

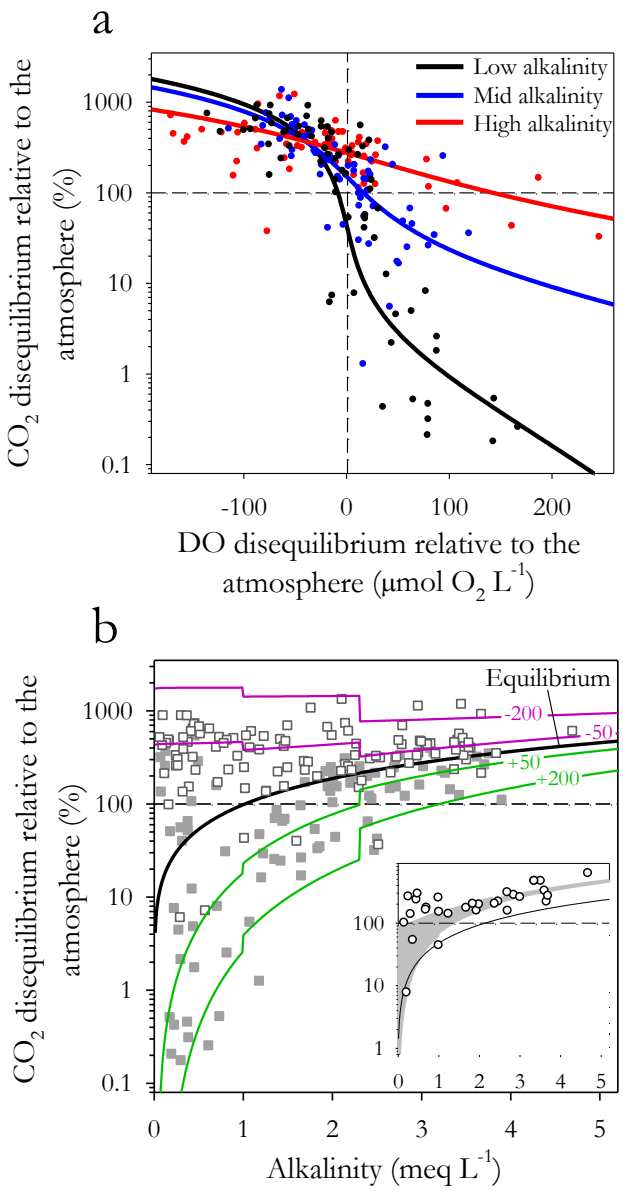

Figure 2. Interplay between alkalinity and NEP shaping CO_2 supersaturation. a, Observed data (dots) and Model 3 results (lines) for the relationship between DO and CO_2 disequilibrium relative to the atmosphere at 25ºC. Groups as in Fig. 1b. **b,** Relationship between alkalinity and CO_2 disequilibrium at 25ºC for samples showing DO supersaturation (filled squares) and undersaturation (open squares). Lines represent realizations of Model 3 for DO equilibrium (bold line) and for different DO disequilibria (color lines, µmol O_2 L^{-1}). *Insert*: Samples at DO saturation within 3% of atmospheric equilibrium (circles) and Model 3 results for the same range (grey area). The thin line is Model 3 solved for DO equilibrium at 10ºC.

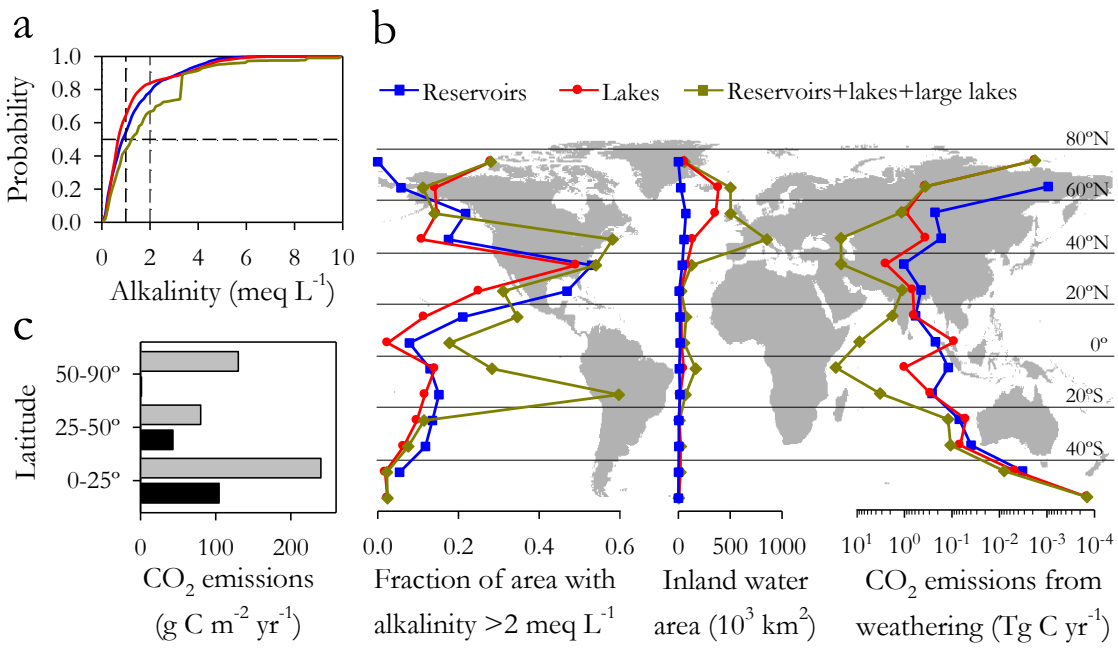

333

334 **Figure 3. Global distribution of lake alkalinity and potential weathering-related**

335 **carbon dioxide emissions from lakes. a,** Cumulative distribution function for alkalinity

336 across the area of reservoirs (blue), lakes (red), and the sum including large lakes (dark

337 green). Dashed lines indicate 1 and 2 meq L^{-1} and probability at 0.5. **b,** Latitudinal

338 distribution of lacustrine systems showing alkalinity > 2 meq L^{-1}, and potential CO_2

339 emissions from DIC^{W}. **c,** Potential emission of CO_2 from DIC^{W} (black bars) compared to

340 calculated global CO_2 emission from lakes and reservoirs (grey bars, ref. 3) in tropical (0-

341 25º), temperate (25-50º), and boreal (50-90º) landscapes.

SUPPLEMENTARY INFORMATION

Carbonate weathering as a driver of carbon dioxide supersaturation in lakes

Rafael Marcé, Biel Obrador, Josep-Anton Morguí, Joan Lluís Riera, Pilar López, Joan Armengol

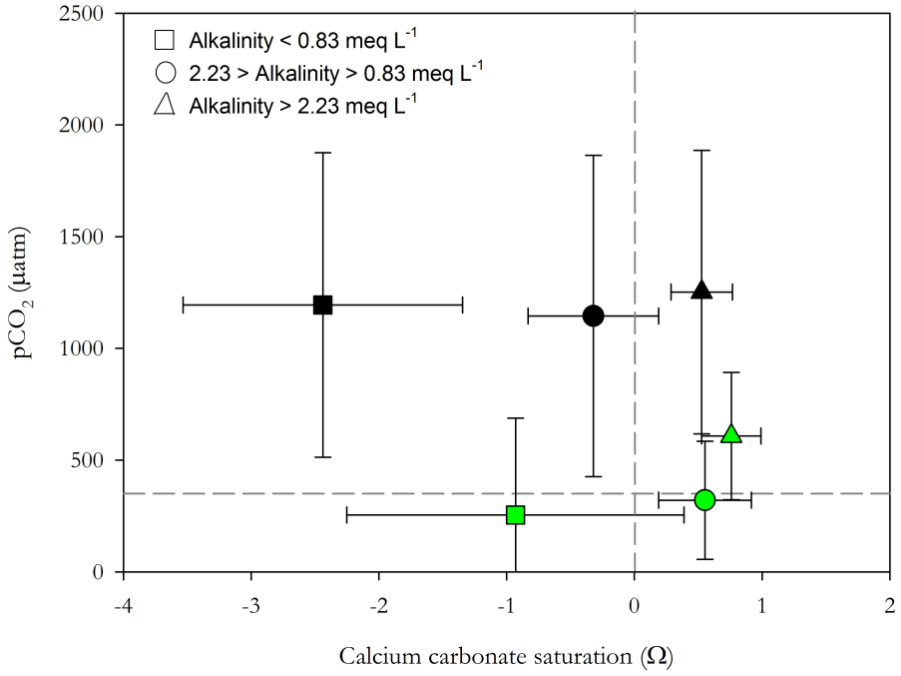

Supplementary Figure 1. Relationship between calcium carbonate saturation in solution and the partial pressure of CO_2 in 101 reservoirs of the Iberian Peninsula. Data were grouped following two criteria: the concentration of alkalinity and the balance of NEP. Green symbols identify those groups of samples showing dissolved oxygen supersaturation (that is, NEP imbalanced towards net autotrophy), while black symbols identify those showing dissolved oxygen undersaturation (i.e., NEP imbalanced towards net heterotrophy). Symbols represent average values for samples grouped following the same alkalinity thresholds as in Fig. 1 (low, mid, and high alkalinity). Bars are standard deviations around the mean value inside each group. Dashed lines indicate pCO_2=350 µatm and Ω=0. Calcium carbonate saturation is an index that expresses whether calcium carbonate in solution is chemically saturated or undersaturated. If Ω>0, calcium carbonate is saturated in solution, and the precipitation of calcite is thermodynamically facilitated. Ω is proportional to calcium concentration times carbonate concentration, and was calculated for each of the 202 samples using observed calcium concentration and carbonate concentration calculated with CO2SYS. Note that at high alkalinity almost all samples were supersaturated in calcium carbonate and CO_2 irrespective of NEP values. By contrast, at low and moderate alkalinity the prevalence of CO_2 supersaturation conspicuously decreased when NEP was imbalanced towards net autotrophy.

SUPPLEMENTARY INFORMATION

Carbonate weathering as a driver of carbon dioxide supersaturation in lakes

Rafael Marcé, Biel Obrador, Josep-Anton Morguí, Joan Lluís Riera, Pilar López, Joan Armengol

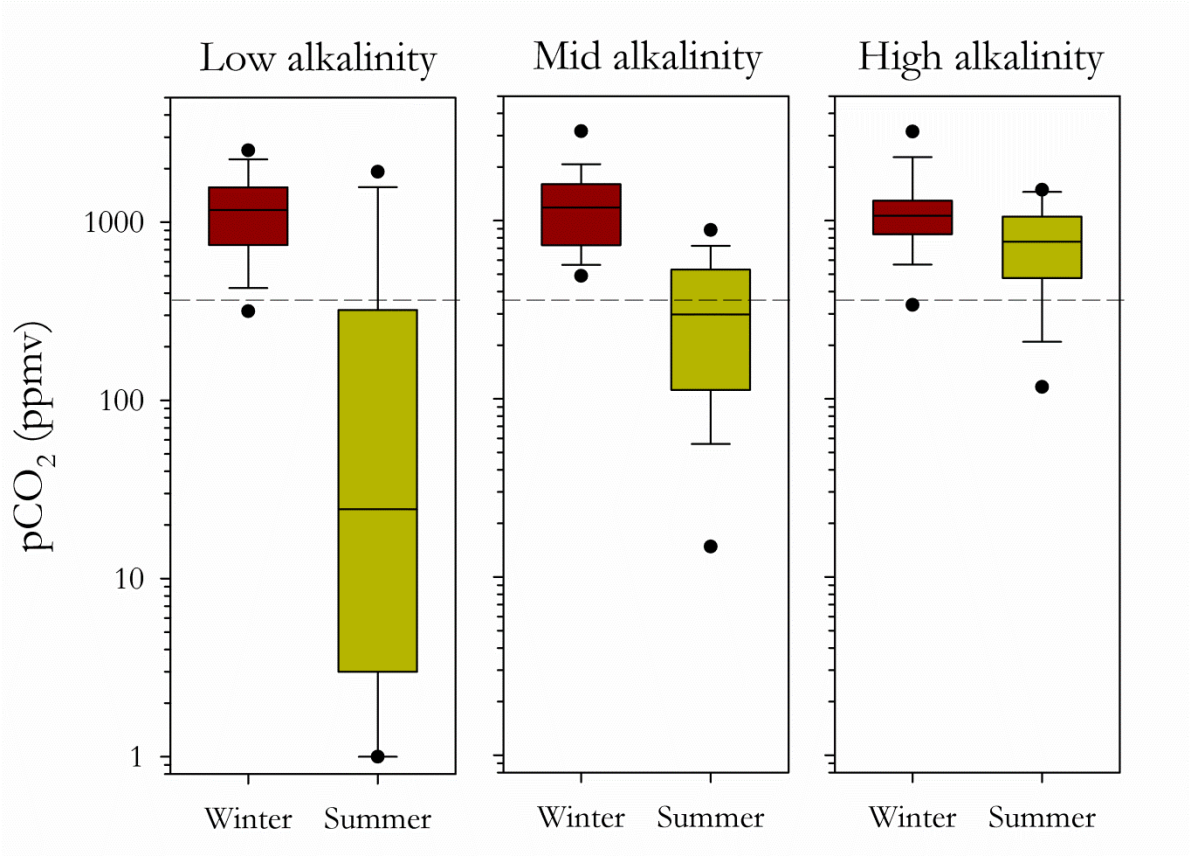

Supplementary Figure 2. Seasonal evolution of CO_2 supersaturation in reservoirs of different alkalinity. The box-whisker plots show the median, and the 10th, 25th, 75th, and 90th percentiles. The points represent the 5th and 95th percentiles. The dashed lines indicate the CO_2 concentration at equilibrium with the atmosphere. The 202 samples were grouped in the same alkalinity groups as in Fig. 1. Note that although differences between seasons were significant in the three sets of reservoirs (Mann-Whitney Rank Sum Test, $P<0.007$), the seasonal shift towards CO_2 undersaturation promoted by primary production during summer is less evident as alkalinity increases. NEP values in Fig. 2a and chlorophyll content across systems (Supplementary Data) clearly indicate that primary production in high alkalinity waters was similar than at low and intermediate alkalinity. Non significant differences in neither total phosphorus, chlorophyll concentration, or DO disequilibrium were actually observed between alkalinity groups (Kruskall Wallis tests, $P>0.05$). Therefore, it is unlikely that the lack of CO_2 undersaturation at higher alkalinity is promoted by a differential primary production.

SUPPLEMENTARY INFORMATION

Carbonate weathering as a driver of carbon dioxide supersaturation in lakes

Rafael Marcé, Biel Obrador, Josep-Anton Morguí, Joan Lluís Riera, Pilar López, Joan Armengol

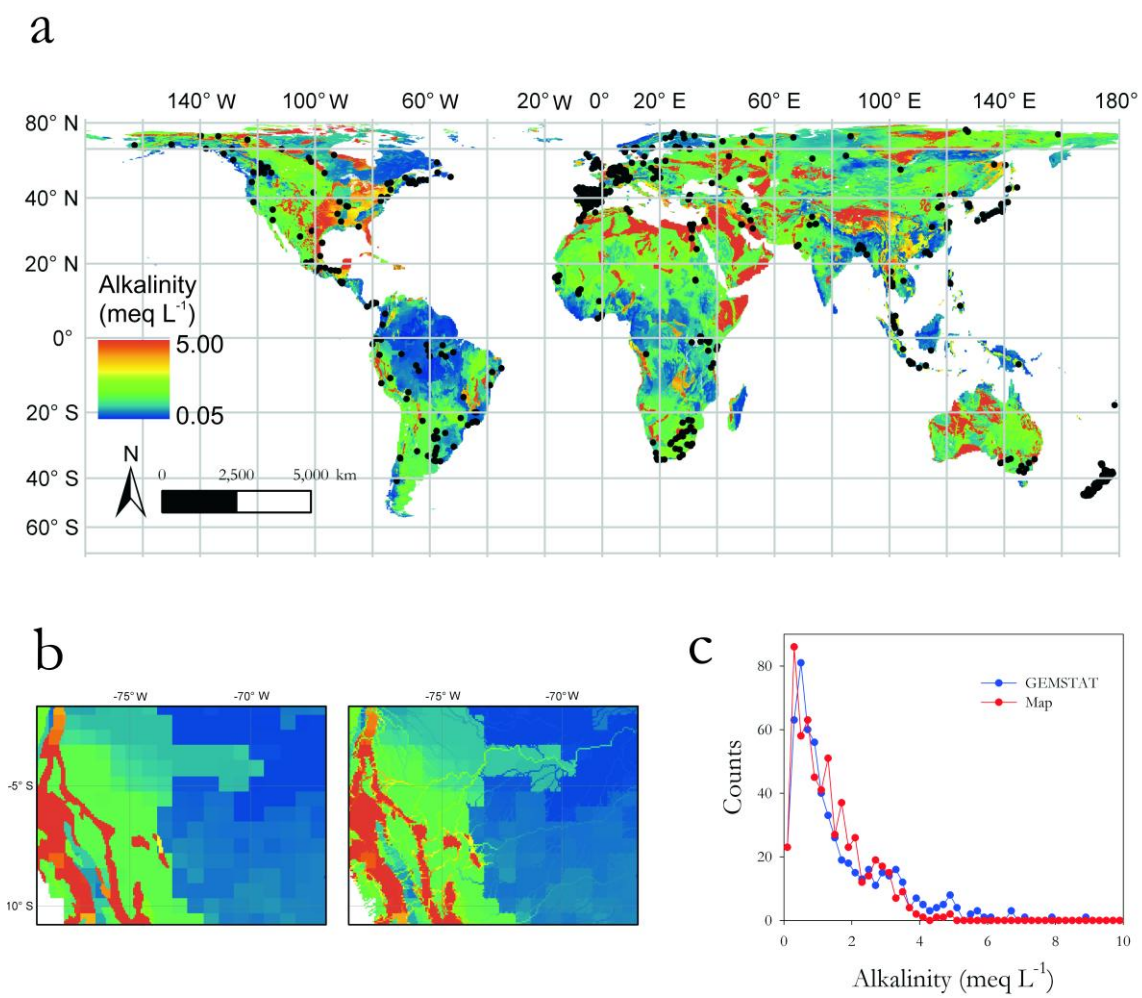

Supplementary Figure 3. Global map of alkalinity in runoff. a, 300 m resolution map for alkalinity in accumulated runoff elaborated in this study, and location of the 584 surface water stations (filled circles) from the GEMSTAT database (www.gemstat.org) used to validate the map. **b,** An example of the comparison between the map of alkalinity in locally generated runoff (left panel) and the final map considering the routing of alkalinity along river networks (right panel). This example is for the Upper Amazonas (the red area roughly corresponds to the Peruvian Andes). Note how the river routing transports alkalinity from the Andes to the downstream Amazonas until inputs of low alkalinity waters dilute the signal. Color legend as in panel **a**. **c,** Comparison between observed and map-generated distributions for mean alkalinity in the 584 GEMSTAT surface water sampling stations showed in panel **a**.

SUPPLEMENTARY INFORMATION

Carbonate weathering as a driver of carbon dioxide supersaturation in lakes

Rafael Marcé, Biel Obrador, Josep-Anton Morguí, Joan Lluís Riera, Pilar López, Joan Armengol

Supplementary Methods

Data collection. We used data collected during a national-wide sampling program during 1987-1988 including 101 reservoirs[15]. This database offers a unique opportunity due to the verifiable accuracy of in-situ chemical analyses, the homogeneity of methods applied across lakes, and the wide range of DIC content and trophic states it covers (Supplementary Table 1 and Supplementary Data). Every system was visited during winter and summer for a total of 202 samples. We measured surface DO concentration by performing Winkler titrations in the field, and DIC and dissolved CO_2 concentrations were estimated from pH (Ross combination electrode Orion 81-04), water temperature, and alkalinity (in situ Gran titration with HCl) along with the dissociation constants for carbonic acid in freshwater systems[31]. CO_2 concentration calculations are very sensitive to errors in pH measurements[2]. In our study this was minimized by the fact that all pH determinations were performed with the same probe and by the same person (J. A. M.) after calibration with buffer solutions in the field. The accuracy of the alkalinity determinations was assessed elsewhere by comparing alkalinity with the ionic balance of the samples[32]. In calculating values for DO, DIC, and CO_2 disequilibrium relative to the atmosphere, elevation effects on atmospheric pressure and a baseline of 350 ppmv CO_2 for 1987-1988 were considered. CO_2 concentrations plotted in Fig. 2 were solved at 25ºC after standardization of pH values at the same temperature to discount the effect of varying water temperatures.

Regression analyses between DO and DIC disequilibrium. To investigate the relationships between DO and DIC disequilibrium relative to the atmosphere in our dataset we performed linear regressions grouping the data considering the 33% and 66% alkalinity percentiles: low alkalinity (n = 67, median = 0.4, range = 0.06-0.83 meq L^{-1}), mid alkalinity (n = 68, median = 1.6, range = 0.88-2.22 meq L^{-1}), and high alkalinity (n = 67, median = 3.0, range = 2.27-4.69 meq L^{-1}). The distribution of some variables inside these three groups showed non-normality. Considering the overly conservative Shapiro-Wilk W test only two out of 6 distributions at play (3 groups for DO and DIC) showed conspicuous deviations from normality (DIC at low and medium alkalinity). We repeated all regression analyses showed in Figure 1b normalizing all variables using Box-Cox transformation. After transformation, all distributions were normal (Shapiro-Wilk W test) except DIC at low alkalinity, that still showed a moderate deviation from normality (skewness=-1.08); and alkalinity, that showed a flat distribution (skewness=0.07) that did not compromise the regression analysis. The analyses showed in Figure 1b but using the transformed variables resulted in an identical result when compared to the analyses using the original variables.

We also performed a factorial regression analysis to test the effect of alkalinity on the DO vs. DIC relationships. Results using original and Box-Cox transformed variables also rendered identical results.

DO disequilibrium as a proxy of NEP. The keystone of our modeling approach is the use of dissolved DO disequilibrium relative to the atmosphere as a surrogate for NEP. This is based on the fact that the time scale for gas equilibration with the atmosphere is large compared to the velocity of metabolic reactions[33]. Therefore, our DO disequilibrium estimates are representative of conditions at the short to medium term, because the supposition of a system closed to the atmosphere would not hold for longer periods (e.g., year). Despite the fact that some recent

works support the use of discrete sampling data to estimate lake NEP[34] there are obvious concerns regarding the magnitude of the diel variations in DO, CO_2, and pH. Consequently, we do not calculate NEP values in mass per volume per time units. However, it is important to note that we do not aim to characterize a water mass in terms of a particular time scale, but rather assess the relationship between carbon and oxygen deviations from equilibrium for a particular moment. In addition, the need for considering spatial heterogeneity in carbon processing in lakes has been increasingly stressed, either in the vertical[35] or horizontal[36,37] dimensions. Spatial heterogeneity appears to be particularly relevant for CO_2 (refs. 38-41) and CH_4 (refs. 42-45) emission estimates from lakes and reservoirs. However, we must note again that our aim is not to characterize the carbon budget of a particular water body, but to assess the relationships between CO_2 and a proxy of NEP in surface water parcels showing contrasted DIC contents. This means that our data should not be considered as representative of the whole system.

All in all, since no temporal and spatial scale can be unequivocally adopted in our calculations, our NEP proxy stays as DO disequilibrium expressed in mass per liter units. Note that this limitation defines our surrogate NEP values as semi-quantitative estimates, because two similar values can indeed be the result of rather different net metabolic rates expressed in the customary mass per volume per time units.

Rationale of the models and the calcification hypothesis. We applied three different models combining different assumptions in a heuristic framework. The aim was to show how the different assumptions explained different patterns in the observed data, in order to guide the reader to the main conclusions of our paper. We understand that this was better accomplished by serially combining our assumptions (i.e., heuristically) in three models, which included the relevant steps of our reasoning.

Although the effects of calcification on the partial pressure of carbon dioxide is a classical topic in oceanography[33] and freshwater research[46], the molar ratios between carbonate precipitation and NEP have been extensively studied in the ocean but they are almost absent in the limnological literature. The molar ratios between carbonate precipitation and NEP used in Model 3 (α in Eq. 2) are lower than those found in marine benthic ecosystems (1.3 for coral reefs[47]), but comparable to ratios measured for marine planktonic assemblages (between 0.2 and 1, ref. 19). Our data come mainly from systems poor in benthic primary producers, hence it is possible that macrophyte-dominated lakes show higher rates of carbonate precipitation to NEP ratios, as has been found in incubation experiments with freshwater macrophytes[18]. In any case, although the assumption of carbonate precipitation to NEP ratios dependent on fixed alkalinity thresholds is clearly not realistic for particular lakes, our results show that it is a reasonable approach when modelling processes across a large population of lakes.

Although our hypothesis that calcite reactions impact the DIC vs. DO disequilibrium is consistent with our results and with the thermodynamic state of calcium carbonate in our samples (Supplementary Figure 1), we acknowledge that we cannot unequivocally assign the observed effect to calcite reactions. Anaerobic metabolic processes like sulfate reduction and denitrification may also impart a similar change in the stoichiometry between DIC and DO[21], although this is unlikely to be responsible for a widespread effect on DIC levels in the surface layer of deep systems like the ones in our dataset. Another process that may be responsible for the observed effect on the DIC vs. DO relationship would be an exchange between water and the atmosphere faster for DO than for CO_2. Actually, the time needed to equilibrate a volume of water with the atmosphere is larger for CO_2 that for DO, due to the effects of the DIC pool on partial pressure of CO_2[48]. Although we cannot discard this effect in our high alkalinity samples, it would be difficult to explain why this process is not affecting the DIC vs. DO relationship in low alkalinity systems as well, because even at low alkalinities the effect of DIC on CO_2 equilibration is not negligible. In any case, although our results are not at odds with the

hypothesis of carbonate precipitation included in Model 3, further research providing direct evidences on the effect of carbonate precipitation and dissolution reactions on lake CO_2 dynamics is required to reach a solid conclusion.

Global map of alkalinity in runoff. The basis for this calculation are the studies of global atmospheric CO_2 consumption by chemical weathering of minerals[49–51]. Those studies collect information on alkalinity fluxes from watersheds of known lithology to build empirical relationships relating runoff and alkalinity fluxes for different lithologies. We assigned different empirical relationships (Supplementary Table 2) to the lithologic classes found in a global lithological map[52] with a resolution of 1 km^2. We used global composite runoff fields[53] to solve the equations for the local generation of alkalinity at every pixel (1 km^2) considering the corresponding lithology, and we converted the figures to alkalinity concentration in meq L^{-1}. All calculations and alignments were performed in ESRI ArcGIS Spatial Analyst. At this step, however, calculations still miss the fact that runoff accumulates along river networks, and this may dramatically change the values of alkalinity in large watersheds draining areas with very different lithologic classes and local runoff generation. To overcome this limitation, we solved the transport of alkalinity along river networks using the Dominant River Tracing (DRT), a global river network database designed to perform macroscale hydrologic calculations[54]. This database merges the HydroSHEDS database[55] with HYDRO1k (USGS, https://lta.cr.usgs.gov/HYDRO1K) to cover high latitude regions not included in the former. We used the flow direction raster at 1/16 of a degree (aprox. 300 m) in ftp://ftp.ntsg.umt.edu/pub/data/DRT to generate an area accumulation raster in ESRI ArcGIS Spatial Analyst (the area accumulation raster at this resolution is incorrect or corrupted in the aforementioned ftp site). After alignment of the different rasters at 300 m resolution (flow direction, area accumulation, local runoff generation, and local alkalinity), the routing of runoff and alkalinity was solved in Matlab 7.2 after exporting all maps in ASCII format

(Supplementary Fig. 3a). The area accumulation raster was used to hierarchically solve calculations, using the flow direction raster to define the cells contributing to each pixel. Alkalinity for accumulated runoff was calculated as the runoff-weighted average of the contributing cells (including the local pixel and considering accumulation effects as calculations progress). Raster maps, ASCII files, and Matlab scripts are available under request to R. M. See Supplementary Fig. 3b for a comparison between the map of alkalinity in locally generated runoff and the same map after considering water routing along river networks.

The final map of alkalinity in accumulated runoff was checked against alkalinity values stored in the GEMSTAT database maintained by UNEP/GEMS/Water Programme (www.gemstat.org). We initially collected 60848 measurement of alkalinity from surface water sampling sites (rivers, lakes, and reservoirs) around the globe, but we finally worked with 55055 measurements from 584 stations (Supplementary Fig. 3a) after discarding several measurements. The main reason to discard measurements was an ambiguous definition of the methodology used to measure alkalinity and of the final units of the results in the database, which coincided with apparently inconsistent results for some stations (extremely wide ranges or unrealistic upper or lower bounds). We calculated the mean alkalinity for each station (the average number of measurements at each station was 99) and compared this value with the alkalinity value of the corresponding pixel in our map of alkalinity in accumulated runoff, using the reported geographic coordinates of the site to extract the value from the map.

The comparison between values from the GEMSTAT database and those extracted from our map gave an average error of 0.26 meq L^{-1}. The distribution of the alkalinity values obtained with the map was very similar to the measured values (Supplementary Fig. 3c), although the map slightly underestimates the prevalence of high alkalinity values. This was expected because our procedure does not account for concentration mechanisms promoted by evaporation, especially relevant in endorheic basins. For this reason the map is not suitable for predicting

alkalinity in saline environments. Another source of error potentially explaining why high alkalinity values are not adequately predicted in our map is the fact that evaporites are always poorly represented in analyses of alkalinity generation from runoff[50–52]. In any case, the overall quality of the results is appropriate for a global analysis focused on global distributions like the one presented here.

Global distribution of alkalinity in lakes and reservoirs. We used two different sources of information to account for lakes and reservoirs. For reservoirs we used the GRAND database[24], while for lakes we used the GLWD database[23]. The polygons of the GRAND database were rasterized at 300 m resolution, and areas corresponding to very large reservoirs (>600 km^2) were removed because the alkalinity map is void inside the margins of very large water bodies. Alkalinity and area values for those very large reservoirs were treated separately in this analysis using data collected from the GEMSTAT database. For lakes we considered the water bodies labeled as lakes in the Levels 1 and 2 of the GLWD database, also rasterized at 300 m resolution. Unfortunately, this includes some reservoirs already present in the GRAND database. To avoid this overlapping, we removed all waterbodies coincident with the GRAND database from our lake map. Very large lakes (>600 km^2) were treated separately following the same procedure as for very large reservoirs. To calculate the areal distribution of alkalinity across lakes and reservoirs we first projected all the layers using the cylindrical equal area Behrmann projection. Then we estimated the areal distribution of alkalinity in lakes and reservoirs by overlapping our map of alkalinity in accumulated runoff with our lake and reservoirs rasters. All analyses were performed in ESRI ArcGIS Spatial Analyst. Results for very large lakes and reservoirs were added to this calculation afterwards. We performed calculations for the entire Earth in 10º latitudinal strips. It is worth mentioning that this analysis does not include the area of very small water bodies not covered by the GRAND and GLWD databases. The area of lakes and reservoirs larger than 0.001 km^2 has been estimated at 3.8 million km^2 (ref. 56), while our lake and reservoir rasters (including very large water bodies) account for 2.5

million km^2. Although the fact that our analysis misses small water bodies is an obvious limitation of our approach, we preferred to restrict our analysis to lakes for which the explicit location was available. In any case, this implies that our estimates of weathering-related CO_2 emissions are indeed conservative figures.

Potential emissions from the supply of alkalinity to lakes and reservoirs. Adopting the assumptions that rock weathering is the main source of alkalinity in surface waters and that this DIC loading reaches lakes and reservoirs without significant equilibration with the atmosphere, we can use DIC^W as defined in this work to calculate the potential emissions of CO_2 in lakes related to chemical weathering in the watershed. DIC^W values across lakes were calculated assuming DIC^W = alkalinity, using our global map of alkalinity in accumulated runoff as the source of alkalinity values. We used values from the GEMSTAT database for very large water bodies (>600 km^2) for which no alkalinity was available from our map. Dissolved CO_2 concentration was calculated from DIC^W using CO2SYS[31] and assuming that the system was not in equilibrium with the atmosphere (i.e., closed system). We used the mean annual air temperature over the continents for the corresponding latitude (NOAA GHCN_CAMS database) to solve calculations in CO2SYS. Although it can be argued that we have applied our findings to natural lakes while our model assumptions have been tested with reservoirs, CO_2 concentrations in lakes and reservoirs older than 10-15 years are comparable[2]. In our dataset, only two reservoirs are less than 15 years old, and average age was 33 years (Supplementary Table 1 and Supplementary Data). We assumed k_{600} = 4 cm hr^{-1} (ref. 3), a value almost identical to recent estimates of the global k_{600} average in lacustrine systems[2]. The actual emissions were calculated by adjusting k and Henry's constant to the mean annual air temperature for the corresponding latitude. Current CO_2 concentration in the atmosphere was assumed at 390 ppmv. We did not consider the effects of chemical enhancement[57] on k values for three reasons. First, chemical enhancement has been neglected in virtually all global assessments of CO_2 emissions from freshwaters, and its use would render our calculations less comparable to other

studies. Second, including chemical enhancement will increase the calculated emissions, and we wanted to keep our calculations as a conservative estimate. Finally and more fundamental, chemical enhancement is more likely to hold in systems showing very high biological activity. However, our calculations are intended to represent the emissions from the supply of weathering related carbon to lakes, without consideration of metabolic activity. Without metabolic activity and considering our assumption that DIC loading reaches lakes and reservoirs without significant equilibration with the atmosphere, pH values cannot rise above 8.5 irrespective of temperature and alkalinity values considered in this paper (calculations performed with CO2SYS). At pH below 8.5, the effect of chemical enhancement on k values is expected to be very small except at unreasonably high temperatures[16,57,58].

We also calculated emissions considering the lower and upper bounds of k_{600} reported in Ref. 2 (2.25 and 7.9 cm hr^{-1}) to assess the sensitivity of the calculated emissions to this parameter. Emissions were substantially sensitive to this parameter in the considered range, because emissions values are linearly dependent on k. Values varied 100% from the central estimate (0.09 P g C yr^{-1}), from 0.05 to 0.17 P g C yr^{-1}. This clearly indicates that reliable regional estimates of k are paramount for a correct assessment of carbon emissions from freshwaters. Emissions were aggregated in 10º latitudinal strips, and compared to previous latitudinal CO_2 emissions estimates[3]. For this comparison, we calculated areal emissions to discount the effect of the different lake and reservoir area considered in Ref. 3 and our work. It should be noted that emissions from DIC^W in this work must be understood as potential emissions. For instance, some high alkalinity systems are highly productive as well[16], showing CO_2 undersaturation.

Supplementary References

31. Pierrot, D., Lewis, E. & Walace, D. W. *Excel Program Developed for CO_2 System Calculations. ORNL/CDIAC-105a.* (Carbon Dioxide Information Analysis Center, Oak Ridge National Laboratory, U.S. Department of Energy, 2006).

32. Riera, J. L. *Regional limnology of Spanish Reservoirs. Relationships between nutrients, seston, and phytoplankton.* (Ph.D. Thesis, University of Barcelona, 1993).

33. Suzuki, A. Combined Effects of Photosynthesis and Calcification on the Partial Pressure of Carbon Dioxide in Seawater. *J. Oceanogr.* **54,** 1–7 (1998).

34. Nielsen, A. *et al.* Daily net ecosystem production in lakes predicted from midday dissolved oxygen saturation: analysis of a five-year high frequency dataset from 24 mesocosms with contrasting trophic states and temperatures. *Limnol. Oceanogr.: Methods* **11,** 202–212 (2013).

35. Obrador, B., Staehr, P. A. & Christensen, J. P. C. Vertical patterns of metabolism in three contrasting stratified lakes. *Limnol. Oceanogr.* **59,** 1228–1240 (2014).

36. Obrador, B. & Pretus, J. L. Carbon and oxygen metabolism in a densely vegetated lagoon: implications of spatial heterogeneity. Limnetica **32,** 321–336 (2013).

37. van De Bogert, M. C., Bade, D. L., Carpenter, S. R., Cole, J. J., Pace, M. L., Hanson, P. C. & Langman, O. C. Spatial heterogeneity strongly affects estimates of ecosystem metabolism in two north temperate lakes. *Limnol. Oceanogr.* **57**, 1689–1700 (2012).

38. Schilder, J. *et al.* Spatial heterogeneity and lake morphology affect diffusive greenhouse gas emission estimates of lakes. *Geophys. Res. Lett.* **40,** doi:10.1002/2013GL057669 (2013).

39. Pacheco, F. S. *et al.* River inflow and retention time affecting spatial heterogeneity of chlorophyll and water–air CO_2 fluxes in a tropical hydropower reservoir. *Biogeosciences Discuss.* **11,** 8531–8568 (2014).

40. Bennington, V., McKinley, G. A., Urban, N. R. & McDonald, C. P. Can spatial heterogeneity explain the perceived imbalance in Lake Superior's carbon budget? A model study. *J. Geophys. Res.* **117,** 1–20 (2012).

41. Teodoru, C. R., Prairie, Y. T. & del Giorgio, P. A. Spatial heterogeneity of surface CO_2 fluxes in a newly created Eastmain-1 reservoir in Northern Quebec, Canada. *Ecosystems* **14,** 28–46 (2011).

42. Maeck, A. *et al.* Sediment Trapping by Dams Creates Methane Emission Hot Spots. *Environ. Sci. Technol.* **47,** 8130−8137 (2013).

43. DelSontro, T., Mcginnis, D. F., Sobek, S., Ostrovsky, I. & Wehrli, B. Extreme methane emissions from a Swiss hydropower reservoir: contribution from bubbling sediments. *Environ. Sci. Tech nol.* **44,** 2415–2425 (2010).

44. DelSontro, T. *et al.* Spatial heterogeneity of methane ebullition in a large tropical reservoir. *Environ. Sci. Technol.* **45,** 9866–9873 (2011).

45. Casper, P., Maberly, S. C., Hall, G. H. & Finlay, B. J. Fluxes of methane and carbon dioxide from a small productive lake to the atmosphere. *Biogeochemistry* **49,** 1–19 (2000).

46. McConnaughey, T. A. *et al.* Carbon budget for a groundwater-fed lake: Calcification supports summer photosynthesis. *Limnol. Oceanogr.* **39,** 1319–1332 (1994).

47. Gattuso, J. P., Allemand, D. & Frankignoulle, M. Photosynthesis and calcification at cellular, organismal and community levels in coral reefs: A review on interactions and control by carbonate chemistry. *Am. Zool.* **39,** 160–183 (1999).

48. Zeebe, R. E. & Wolf-Gladrow, D. *CO_2 in Seawater: Equilibrium, Kinetics, Isotopes*. Elsevier, 360 pp. (2001).

49. Suchet, P. A., Probst, J.-L. & Ludwig, W. Worldwide distribution of continental rock lithology: Implications for the atmospheric/soil CO_2 uptake by continental weathering and alkalinity river transport to the oceans. *Global Biogeochem. Cycles* **17,** 14 (2003).

50. Hartmann, J., Jansen, N., Dürr, H. H., Kempe, S. & Köhler, P. Global CO_2-consumption by chemical weathering: What is the contribution of highly active weathering regions? *Glob. Planet. Change* **69,** 185–194 (2009).

51. Jansen, N. *Chemical rock weathering in North America as source of dissolved silica and sink of atmospheric CO_2.* (Ph.D. Thesis, University of Hamburg, 2010).

52. Dürr, H. H., Meybeck, M. & Dürr, S. H. Lithologic composition of the Earth's continental surfaces derived from a new digital map emphasizing riverine material transfer. *Global Biogeochem. Cycles* **19,** GB4S10 (2005).

53. Fekete, B. M., Vörösmarty, C. J. & Grabs, W. High-resolution fields of global runoff combining observed river discharge and simulated water balances. *Global Biogeochem. Cycles* **16,** 1042 (2002).

54. Wu, H. *et al.* A new global river network database for macroscale hydrologic modeling. *Water Resour. Res.* **48,** W09701 (2012).

55. Lehner, B., Verdin, K. & Jarvis, J. New global hydrograph derived from spaceborne elevation data. *Eos* **89,** 93–94 (2008).

56. Mcdonald, C. P., Rover, J. A., Stets, E. G. & Striegl, R. G. The regional abundance and size distribution of lakes and reservoirs in the United States and implications for estimates of global lake extent. *Limnol. Oceanogr.* **57,** 597–606 (2012).

57. Wanninkhof, R. & Knox, M. Chemical enhancement of CO_2 exchange in natural waters. *Limnol. Oceanogr.* **41,** 689–98 (1996).

58. Portielje, R. & Lijklema, L. Carbon dioxide fluxes across the air-water interface and its impact on carbon availability in aquatic systems. *Limnol. Oceanogr.* **40,** 690-699 (1995).